Submitted to the XVIII Int. Symposium on Lepton Photon Interactions,
Hamburg 1997

BOUNDS ON QCD INSTANTONS FROM HERA

T. Carli[1] and M. Kuhlen[2]

Max-Planck-Institut für Physik
Werner-Heisenberg-Institut
Föhringer Ring 6
D-80805 München
Germany

Abstract

Signals for processes induced by QCD instantons are searched for in HERA data on the hadronic final state in deep-inelastic scattering. The maximally allowed fraction of instanton induced events is found at 95% confidence level to be on the percent level in the kinematic domain $10^{-4} \lesssim x \lesssim 10^{-2}$ and $5 \lesssim Q^2 \lesssim 100$ GeV^2. The most stringent limits are obtained from the multiplicity distributions.

[1]carli@desy.de
[2]kuhlen@desy.de

1 Introduction

The standard model contains processes which cannot be described by perturbation theory, and which violate classical conservation laws like baryon and lepton number in the case of the electroweak and chirality in the case of the strong interaction [1]. Such anomalous processes are induced by instantons [2]. At HERA, which collides 27.5 GeV positrons on 820 GeV protons, QCD instantons may lead to observable effects in the hadronic final state in deep-inelastic scattering (DIS) [3, 4, 5, 6, 7, 8, 9, 10]. Instantons isotropically decay into a high multiplicity state, consisting of gluons and all quark flavours which are kinematically allowed in each event (see Fig. 1). One expects therefore a densely populated region in rapidity, other than the current jet, which is homogeneously distributed in azimuth. The presence of strangeness and charm provides an additional signature. From the analysis of K^0 yields [11] and multiplicity distributions [12] the H1 collaboration has put first limits on instanton production for Bjorken $x > 0.001$. They allow at most a few per cent admixture of instanton events to normal DIS events.

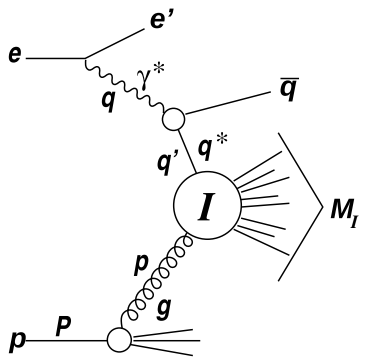

DIS variables:
$Q^2 = -q^2$
$x = Q^2 /(2P \cdot q)$
$W^2 = Q^2 (1-x)/x$

Variables of instanton sub-process:
$Q'^2 = -q'^2$
$x' = Q'^2 /(2\, p \cdot q')$
$M_I^2 = Q'^2 (1-x')/x'$

Figure 1: Diagram of an instanton induced process in DIS, where a virtual photon with 4-momentum q emitted from the incoming electron fuses with a gluon with 4-momentum p emitted from the proton with 4-momentum P. The virtual quark q^* entering the instanton subprocess has 4-momentum q'. These 4-momenta define the DIS variables x, Q^2, and x' and Q'^2 characterizing the instanton subprocess. W is the invariant mass of the hadronic final state, and M_I the invariant mass of the hadrons emerging from the instanton subprocess.

We have investigated systematically the sensitivity of all available HERA hadronic final state data to instanton production. In this paper we analyze the data which are most sensitive to instanton production, namely the multiplicity distributions [12], the transverse energy flows [13], and hard particle production [14]. We derive limits on instanton production, improving existing limits by an order of magnitude, and extend them into previously uncovered kinematic regions.

The paper is organized as follows: in chapter 2 the details of the Monte Carlo simulation of the hadronic final state are given, in chapter 3 the instanton phenomenology is described, in chapter 4 we discuss the HERA data in the light of instanton production and present the new bounds, and finally conclude in chapter 5.

2 Monte Carlo simulation

Predictions for the hadronic final state in normal and in instanton induced DIS events are extracted from Monte Carlo generators, which model the interaction. They incorporate QCD evolution and parton radiation in different approximations and utilize phenomenological models for the non-perturbative hadronization phase.

2.1 Standard QCD models

The QCD Monte Carlo simulation program ARIADNE [15] uses the QCD matrix elements up to first order of the strong coupling constant α_s, with additional multi-gluon emissions from a chain of independently radiating dipoles formed by the colour charges [16]. The hadronization is performed with the LUND string model [17] as implemented in JETSET [18]. ARIADNE provides an excellent description of all available HERA data on the hadronic final state in DIS [19].

2.2 Instanton Monte Carlo

The Monte Carlo event generator QCDINS [20, 21] is used to model the hadronic final state of instanton induced processes in DIS. It also predicts the total cross section in a restricted phase space region.

Events induced by QCD instantons predominantly invoke a quark-gluon fusion process[3] as depicted in Fig. 1. The total cross section is given by a convolution of the probability to find a gluon in the proton $P_{g/p}$, the cross section $\sigma^{(I)}_{q^*g}(x', Q'^2)$ of the instanton induced subprocess and the probability that a photon splits into a quark-antiquark pair in the instanton background $P^{(I)}_{q^*/\gamma^*}$ [9, 8]. Besides the squared transverse momentum transfer Q^2 and the Bjorken-x scaling variable, this scattering process is characterized by Q'^2, the virtuality of the quark (q^*), and x', the Bjorken scaling variable associated with the q^*g subprocess (see Fig. 1 for definition).

The cross section of the instanton induced subprocess is given by [9]:

$$\sigma^{(I)}_{q^*g}(x', Q'^2) \approx \frac{\Sigma(x')}{Q'^2} \left(\frac{4\pi}{\alpha_s(\mu(Q'))} \right)^{\frac{21}{2}} \exp \left(\frac{-4\pi}{\alpha_s(\mu(Q'))} F(x') \right) \tag{1}$$

where $\Sigma(x')$ and $F(x')$ are known functions of x' as long as x' is not too small, say $x' \gtrsim 0.2$. $\mu(Q')$ is the renormalisation scale. $F(x')$ modifies the exponential

[3] Quark induced processes have not yet been taken into account and are expected to be of minor importance.

suppression factor $\exp(-4\pi/\alpha_s)$ typical for tunneling processes and has its origin in multi-gluon emissions at high energies [22]. $F(x')$ is 1 for $x' = 1$ and is decreasing towards small x'. For $x' \approx 0.2$, $F(x')$ is ≈ 0.5. The assumed expression for $F(x')$ is considered to be a reasonable estimate for $x' \gtrsim 0.2$. The extrapolation to lower values of x' is unreliable due to inherent ambiguities [9]. Moreover Q'^2 has to be large enough ($Q'^2 \gtrsim 25$ GeV^2) to allow (instanton) perturbation theory to be applied. Another source of uncertainty comes from a residual renormalisation scale dependence.

The total instanton induced q^*g cross section decreases with increasing Q'^2 and exponentially grows with decreasing x'. Since the center of mass energy of the q^*g system is $M_I = \sqrt{Q'^2\,(1-x')/x'}$, the expected event topology will be strongly influenced by these two variables. x' and Q'^2 are in principle observables measurable from the hadronic final state. Here we consider instanton events which are produced above various x' and Q'^2 cut-offs.

From the instanton subprocess, n_f quark-antiquark pairs and n_g gluons are being emitted isotropically in the q^*g center of mass system. n_f is the number of flavours which are kinematically allowed[4]. Each event thus contains quarks of all kinematically allowed flavors. The number of gluons n_g in the instanton subprocess is generated according to a Poisson distribution and is ≈ 2 for $x' \gtrsim 0.2$ and $Q'^2 \gtrsim 25$ GeV^2[4, 21].

The flavour of the current quark (produced by the splitting of the photon in the instanton background) is chosen at random. Its 4-vector is reconstructed from x and Q^2 using a Sudakov decomposition. The cross sections are calculated with massless quarks, but the generated final state quarks are massive.

After assembling the hard instanton induced subprocess, QCDINS allows for further gluon emission in the leading-logarithm approximation simulated with a coherent parton branching algorithm as implemented in HERWIG [23]. The transition from partons to the observable hadrons is performed with the cluster fragmentation model [24], where the primary hadrons are produced from an isotropic two body decay of colour singlet parton clusters. QED radiation is not implemented. The published data used in this analysis had been corrected for QED radiation.

3 The instanton induced final state

We study DIS events in the center of mass system (CMS), of the incoming proton and the virtual boson, i.e. the CMS of the hadronic final state with invariant mass W. Longitudinal and transverse quantities are calculated with respect to the virtual boson direction (defining the $+z$ direction).

In this analysis we concentrate on the instanton production scenario with $x' > 0.2$ and $Q'^2 > 25$ GeV^2 as cut-off parameters. In this phase space region the in-

[4]In this analysis the maximally allowed number of flavours was set to 5. The mean multiplicity of charged particles is reduced by 10% when only 4 flavors are considered.

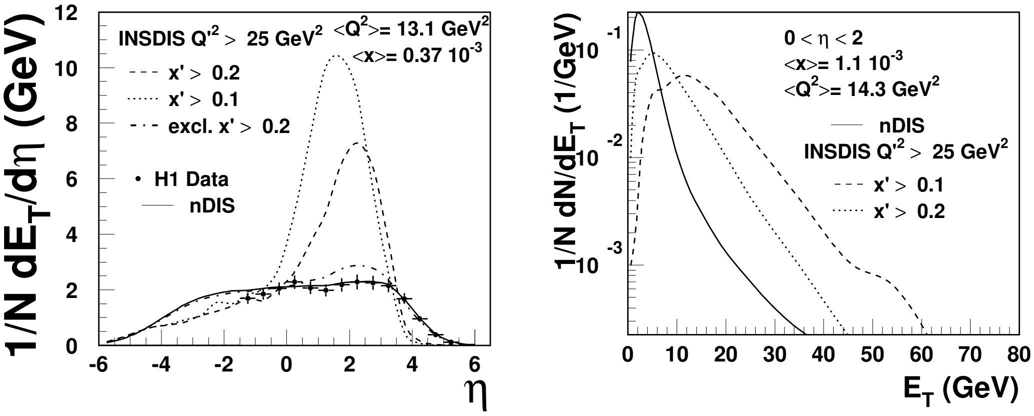

Figure 2: **a)** The transverse energy flow E_T as a function of pseudorapidity η in the hadronic CMS. The proton remnant direction is to the left. The standard QCD model (nDIS=ARIADNE) and different instanton scenarios are confronted with the H1 data [13]. The excluded scenario with an instanton fraction $f_I > 11.8\%$ for $x' > 0.2$ is indicated. **b)** The E_T distribution, where the transverse energy is measured in the CMS rapidity bin $0 < \eta < 2$, for two instanton scenarios, and the standard QCD model (nDIS). The plots are normalized to the total number of events N.

stanton cross section calculation is considered to be relatively safe [9]. To investigate the sensitivity to x' and Q'^2 we also consider scenarios where either the event topology is spectacular (low x', large Q'^2), or the cross section can be potentially large (low x').

In the rest frame of the instanton induced subprocess partons are isotropically emitted. This multi-parton state consists of gluons and all quark flavours which are kinematically allowed. In the CMS the hadrons emerging from the instanton subprocess occupy a homogeneous band in pseudorapidity[5] [4]. As an example, Fig. 2a shows the flow of hadronic transverse energy (E_T) as a function of pseudorapidity η in a certain x -Q^2 bin. The height and position of the instanton band depends on the chosen production scenario. For lower x' the instanton band gets stronger and moves towards the remnant. In normal DIS events on average an E_T of 2 GeV per unit pseudorapidity is observed. In instanton induced events, the average E_T may go up to 10 GeV per η unit for low x'. A possible search strategy could involve the E_T distribution in a selected rapidity band (Fig. 2b), looking for high E_T events in the tail of the distribution.

The same effect can be seen in the pseudorapidity distribution of charged particles, see Fig. 3a. Instanton events are characterized by a large particle density localized in rapidity. In normal DIS events there are about 2 charged particles per unit of rapidity [14], while in instanton events there are up to 10 charged particles per unit of rapidity for a low x' cut-off, and somewhat less for a high x' cut-off.

[5]The pseudorapidity η is defined as $\eta = -\ln\tan\theta/2$, where θ is the angle of the hadron with respect to the virtual photon direction in the hadronic center of mass frame.

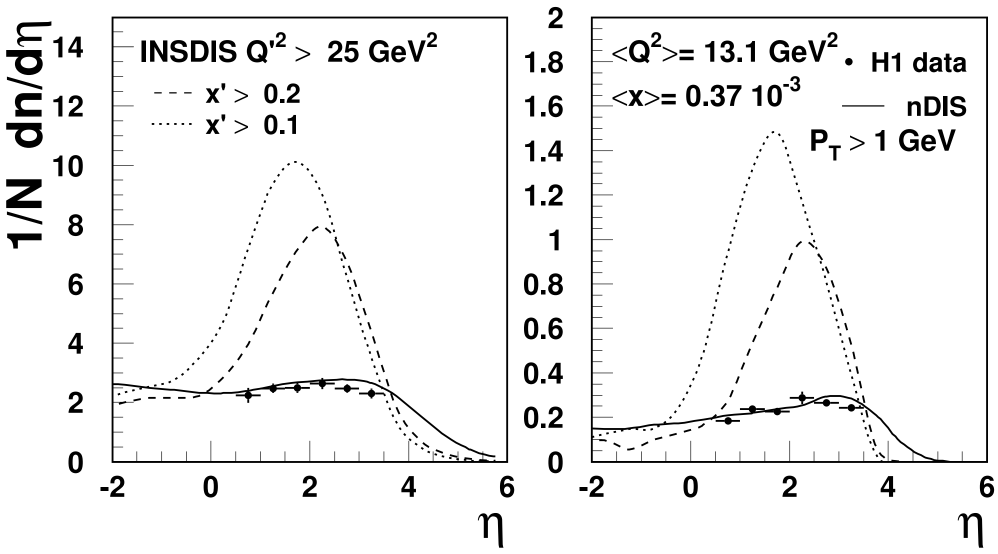

Figure 3: The rapidity distribution of charged particles in the hadronic CMS for **a)** all charged particles, and **b)** charged particles with $p_T > 1$ GeV. The proton remnant direction is to the left. The standard QCD model (nDIS=ARIADNE) and different instanton scenarios (INSDIS) are confronted with the H1 data [14]. The plots are normalized to the total number of events N. Both plots are for $\langle x \rangle = 0.37 \cdot 10^{-3}$ and $\langle Q^2 \rangle = 13.1$ GeV^2.

The production of instanton induced events would be signaled by events with abnormally large particle multiplicity. In Fig. 4 the distribution of charged particle multiplicities is shown. A significant fraction of the instanton events would lead to charged multiplicities which are very unlikely to be found in normal DIS events, as predicted from standard QCD Monte Carlos. Higher multiplicities are produced for lower x' and larger Q'^2 due to the larger M_I. For small x' also the transverse momentum (p_T) spectrum of charged particles is somewhat harder for instanton events than for normal DIS events (see Fig. 4b), owing to the many semi-hard partons emerging from the instanton subprocess. This is also reflected in the multiplicity flow of hard particles ($p_T > 1$ GeV), see Fig. 3b. For low x', there are about 1.4 hard charged particles per unit rapidity in the instanton band, while for normal DIS only 0.2 would be expected on average.

The distributions presented so far are compared to actual HERA measurements [12, 14]. The data can be described relatively well by standard QCD models. This fact allows to place bounds on instanton production, which will be discussed in the next section.

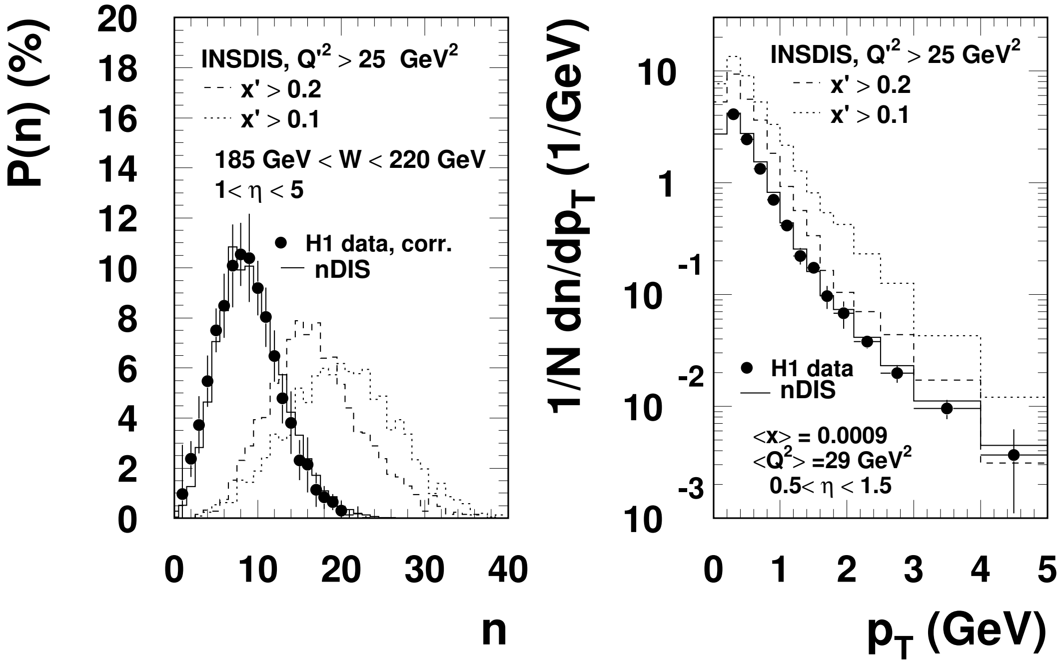

Figure 4: **a)** The probability distribution $P(n)$ of the charged particle multiplicity n from the CMS pseudorapidity range $1 < \eta < 5$ for events with 185 GeV $< W <$ 220 GeV. Shown are the unfolded H1 data [12], the expectation from a standard DIS model (nDIS=Ariadne), and the predictions for instanton events with different cut-off scenarios. **b)** The transverse momentum spectrum (p_T) of charged particles in the pseudorapidity range $0.5 < \eta < 1.5$. Shown are the expectations for normal DIS (nDIS) and for instanton events (INSDIS), and the measurement from H1 [14]. The plot is normalized to the total number of events N.

4 Limits on instanton production

4.1 Limits from shape comparisons

To determine an upper limit on the instanton induced production cross-section, it is assumed that the considered measured observable results from an admixture of instanton induced (INSDIS) to normal DIS (nDIS) events with a fraction f_I. From a χ^2 test, comparing $f_I \cdot \mathrm{INSDIS} + (1 - f_I) \cdot \mathrm{nDIS}$ events with the data, the maximally allowed fraction (f_{lim}) of instanton events in the data is deduced at 95% confidence level (C.L.). The upper bound on the instanton production cross-section (σ_{lim}) is calculated from f_{lim}, the number of generated instanton and normal DIS events and the known total DIS cross-section in the considered kinematic region.

Among all investigated observables in the hadronic final state of DIS events, the transverse energy flow ($\mathrm{d}E_T/\mathrm{d}\eta$), the flow of hard charged particles ($\mathrm{d}n/\mathrm{d}\eta$ for $p_T > 1$ GeV), and the transverse momentum spectra of charged particles in a restricted rapidity region $0.5 < \eta < 1.5$ give the best sensitivity in the analysis where shapes of data are compared to Monte Carlo simulations. An example of an instanton admixture to normal DIS which can be excluded at 95% C.L. is shown in Fig. 2.

In Fig. 5 the results for instantons with $x' > 0.2$ and $Q'^2 > 25$ GeV^2 are summarized. For $10^{-4} \lesssim x \lesssim 10^{-2}$ and $10 < Q^2 < 50$ GeV^2, instanton fractions f_I between $5 - 10\%$ can be excluded from the E_T flow data. This corresponds to cross-section limits of $\approx 200 - 800$ pb. The best limits are reached in the domain of higher x and Q^2. The limits obtained from the charged particle η and p_T spectra are of comparable order as the ones obtained from the E_T flows. When going into the low x' region ($x' > 0.1$), where the cross-section calculation is doubtful but the event topology more distinct, somewhat better $f_{\rm lim}$ values of about $3 - 8\%$ can be reached. Increasing the Q'^2 cut-off to 100 GeV^2 has a similar effect. However, the cross-section predicted by the instanton Monte Carlo drops by a factor of 10, such that the gain in sensitivity due to the more distinct event topology is not big enough to compensate for the falling instanton cross-section.

Systematic uncertainties can be investigated by varying options in the standard DIS Monte Carlo, like the parameterization of the proton structure function F_2 or parameters associated with the hadronisation model. Among the F_2 parameterizations from Martin, Roberts and Stirling [25] (MRS-H), from the CTEQ collaboration [26] (CTEQ-4d) and from Glück, Reya and Vogt [27] (GRV-94 HO), MRS-H turned out to give the most conservative limits and was therefore chosen to determine σ_{lim} and f_{lim}. Using other structure function parameterizations leads to up to 50% lower cross-section limits and, in exceptional cases, they are even lowered by a factor of 2. Replacing the JETSET hadronisation parameters by sets which have been tuned to LEP data [28] alters the cross-section limits by about 20%.

One has to keep in mind that this method relies on the assumption that the used standard QCD Monte Carlo is a good model of standard QCD effects without instantons. Though it gives an excellent description of the available hadronic final state data over the full kinematic plane, the true QCD dynamics, in particular at small x, is still under debate. The method discussed in the following section does not rely on this assumptions.

4.2 Limits from multiplicity distributions

The most sensitive data to instanton induced processes are the multiplicity distributions $P(n)$ giving the probability to produce n hadrons in an event. Instanton events are characterized by abnormally large hadron multiplicities n. H1 has presented the observed charged particle multiplicity distribution in the CMS pseudo-rapidity interval $1 < \eta < 5$ for four different regions of W [12]. Here we exploit the fact that events above a certain multiplicity $n_{\rm max}$ were not observed to place limits on instanton production [6].

[6] H1 already derived a limit on instanton production by looking for a deviation from the multiplicity distribution for normal DIS events, assumed to be a negative binomial distribution, for multiplicities $n < n_{\rm max}$ [12].

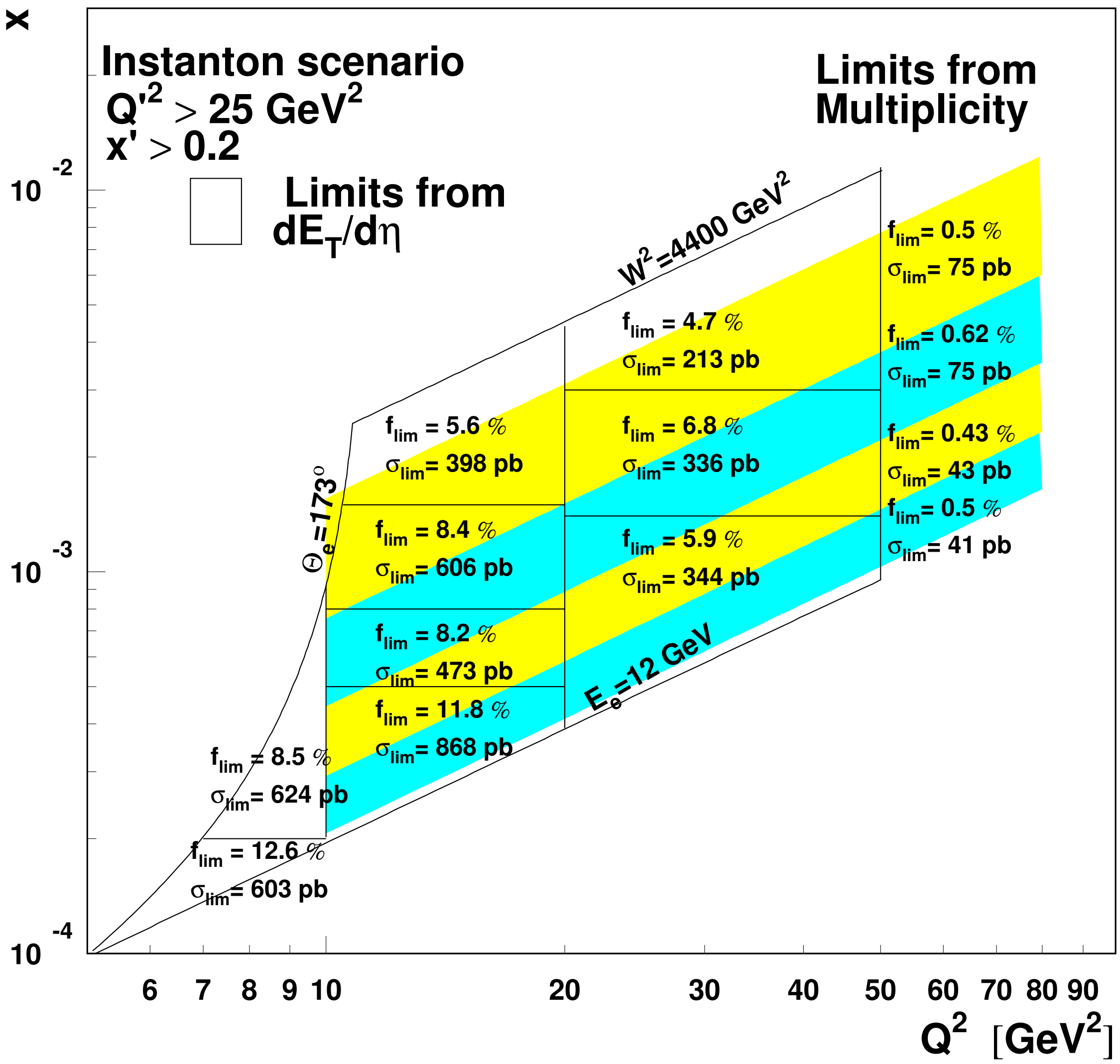

Figure 5: Limits on instanton production with $Q'^2 > 25$ GeV^2 and $x' > 0.2$. The cross-section limits ($\sigma_{\rm lim}$) together with the maximally allowed instanton fraction $f_{\rm lim}$ are shown in the (x,Q^2) plane obtained from the dE_T/dη (open fields) and multiplicity analysis (shaded fields) with their numbers at the right edge.

The observation of no events above $n_{\rm max}$ has to be compared to the expectation from instanton events. We define the instanton search region in the multiplicity distribution by requiring $n > n_{\rm max}$. The fraction of instanton events satisfying the multiplicity cut $n > n_{\rm max}$ gives the instanton efficiency ε_I

$$\varepsilon_I(n_{\rm max}) = \sum_{n>n_{\rm max}} P_I(n) \qquad (2)$$

kinematic bin	W(GeV)	$\langle x\rangle/10^{-3}$	$\langle Q^2\rangle$ (GeV^2)	N	$n_{\max}$
A	80-115	2.43	22.9	16680	20
B	115-150	1.33	23.2	14983	24
C	150-185	0.84	23.3	12191	25
D	185-220	0.58	23.5	9255	26

Table 1: Summary of H1 multiplicity data [12] which are used in this analysis. The data correspond to an integrated luminosity of 1.3 pb^{-1}.

and is calculated with the instanton generator.

By comparing the observed and the unfolded data multiplicity distribution from H1 we conclude that they are very similar; if anything, the raw distribution is slightly broader than the unfolded distribution. Therefore the true instanton efficiency including detector effects, is very similar, and if anything, slightly larger than our estimate from the instanton generator, which neglected detector effects. Our assumption on ε_I is therefore conservative. We assume however, that the H1 acceptance is not biased against high multiplicity events. This appears reasonable as H1 imposes only very loose cuts in the DIS event selection [12]. For example, the requirement of a reconstructed event vertex from charged tracks should introduce losses only for low multiplicity events. Also, tracks from instanton events are produced isotropically, avoiding very dense track configurations with potential problems due to the limited double track resolutions in the central drift chamber.

The same line of reasoning applies to QED radiative effects, because for the unfolded distributions also radiative corrections had been applied. Furthermore, with the given event selection and kinematic reconstruction method, the kinematic distributions are little affected by QED radiation [29].

The 95% C.L. limit $f_{\rm lim}$ on the fraction of instanton events in a given DIS event sample f_I is then calculated from the 95% C.L. upper limit corresponding to zero events seen (i.e. three), ε_I, and the total number of DIS events observed N (given by H1):

$$f_I < f_{\rm lim} = \frac{3/\varepsilon_I}{N} \quad (95\%\ \text{C.L.}) \tag{3}$$

This fractional limit can be converted into a cross-section limit:

$$\sigma_I < \sigma_{\rm lim} = f_{\rm lim} \cdot \sigma_{\rm DIS} \tag{4}$$

Here $\sigma_{\rm DIS}$ is the DIS cross-section calculated for the kinematic bin from a recent parameterization of the parton density functions [25] which fits the HERA structure function data [30, 31]. The H1 data used are summarized in table 1, and the results from this analysis are presented in table 2 and Fig 5. Contrary to previous analyses [12, 11] and the other results discussed in this paper, these results do not depend on models for the standard DIS process, because no background had to be subtracted.

$Q'^{\,2} > 25\ \mathrm{GeV}^2$, $x' > 0.1$					
kinematic bin	σ_{DIS} (pb)	ε_I	f_{lim}	σ_{lim} (pb)	extrapolated σ_I (pb)
A	14800	0.08	0.0023	34	900
B	12200	0.07	0.0029	35	1400
C	9900	0.13	0.0020	20	1400
D	8300	0.19	0.0017	15	1300
$Q'^{\,2} > 25\ \mathrm{GeV}^2$, $x' > 0.2$					
kinematic bin	σ_{DIS} (pb)	ε_I	f_{lim}	σ_{lim} (pb)	predicted σ_I (pb)
A	14800	0.04	0.0050	75	2.6
B	12200	0.03	0.0062	75	3.1
C	9900	0.06	0.0043	43	2.9
D	8300	0.07	0.0050	41	2.7

Table 2: Limits on instanton production from the analysis of the H1 multiplicity data compared to predicted and extrapolated instanton production cross section. The prediction is only considered reliable for $x' \gtrsim 0.2$.

The predicted instanton induced cross-sections crucially depend on the x' and Q' cut-offs, and on the renormalisation and factorization scheme chosen at this level of approximation, varying by orders of magnitudes for the chosen scenarios. ε_I and the derived instanton limits depend much less upon the instanton kinematics, they typically vary by a factor 2 or 3. These findings are summarized in table 3. Experimentally favorable are large Q'^2 and low x', because that results in a large instanton "mass". The instanton induced cross-section decreases with increasing Q'^2 and x'. For lower x' the cross-section calculation becomes unreliable, because higher order interactions are expected to dampen the growth in cross-section. The predictions quoted here are calculated with the instanton Monte Carlo, which extrapolates also into the unreliable region of small x' and Q'^2.

For a theoretically "safe" scenario, $Q'^2 > 25\ \mathrm{GeV}^2$ and $x' > 0.2$ [9], the limits are still roughly a factor 20 away from the predicted cross-section (see Fig. 6). When the x' cut-off is lowered to 0.1, the instanton efficiency improves by roughly a factor two, and the extrapolated instanton cross-section increases by a factor ≈ 500. The data clearly rule out such a large instanton cross-section and thus provide a constraint for the behavior of the functions $F(x')$ and $\Sigma(x')$ (see equation 1) in the theoretically uncertain region at small x'. Qualitatively the same features are observed for the other Q'^2 scenarios with a very low and a very high cut-off.

5 Conclusions

The observation of instanton effects in DIS events at HERA would be a novel, non-perturbative manifestation of QCD and would furthermore provide valuable indirect information about $B + L$ violation in the multi-TeV region induced by

Instanton cross-section (pb) limit/predicted		bin A		bin B		bin C		bin D	
		$\sigma_{\rm lim}$	σ_I	$\sigma_{\rm lim}$	σ_I	$\sigma_{\rm lim}$	σ_I	$\sigma_{\rm lim}$	σ_I
$Q'^2 > 0.05$ GeV^2	$x' > 0.1$	43	1500	49	2200	22	2300	17	2000
$Q'^2 > 0.05$ GeV^2	$x' > 0.2$	97	7.1	124	7.3	66	6.9	51	5.7
$Q'^2 > 25$ GeV^2	$x' > 0.1$	34	930	35	1400	20	1400	15	1300
$Q'^2 > 25$ GeV^2	$x' > 0.2$	75	2.6	75	3.1	43	2.9	41	2.7
$Q'^2 > 100$ GeV^2	$x' > 0.1$	31	140	23	270	12	300	10	330
$Q'^2 > 100$ GeV^2	$x' > 0.2$	28	0.3	23	0.5	13	0.5	13	0.4

Table 3: Cross-section limit $\sigma_{\rm lim}$ and predicted/extrapolated cross-section σ_I for the different (x',Q'^2) scenarios. The prediction is only considered reliable for $x' \gtrsim 0.2$.

electroweak instantons. The distinct event topology of instanton induced events allows to discriminate them from normal DIS events. Using existing HERA data on the hadronic final state corresponding to an integrated luminosity of $\mathcal{O}(1\ \mathrm{pb}^{-1})$, the maximally allowed fraction of instantons in DIS is found to be of $\mathcal{O}(1\%)$ for $80 < W < 220$ GeV and $x' > 0.2$ and $Q'^2 > 25$ GeV^2. In this phase space region the predicted instanton fraction is $\approx 0.01 - 0.02\%$, i.e. still below the level excluded by existing HERA data. Dedicated instanton searches employing more elaborate search strategies and higher luminosities will help to test the prediction of the cross-section in future.

6 Acknowledgements

We would like to thank A. Ringwald and F. Schrempp for many inspiring discussions on the instanton theory, P. van Mechelen for discussions on multiplicity distributions, and our summer students B. Koblitz and C. Tesch for their help. We also thank J. Gayler, A. Ringwald and F. Schrempp for their critical reading of the manuscript. M. K. wishes to thank the Deutsche Forschungsgemeinschaft for their support.

References

[1] G. 't Hooft, Phys. Rev. Lett. 37 (1976) 8; Phys. Rev. D14 (1976) 3432.

[2] A. Belavin, A. Polyakov, A. Schwarz and Yu. Tyupkin, Phys. Lett. B59 (1975) 85.

[3] I.I. Balitskii and V.M. Braun, Phys. Lett. B314 (1993) 237.

[4] A. Ringwald and F. Schrempp, DESY 94-197, hep-ph/9411217, Proc. of Int. Sem. "Quarks 94", Vladimir, Russia, 1994, p. 170.

[5] M. Gibbs, A. Ringwald and F. Schrempp, DESY 95-119, hep-ph/9506392, Proc. of the Workshop on "Deep Inelastic Scattering and QCD" - DIS95, Paris 1995, eds. JF. Laporte and Y. Sirois, p. 341.

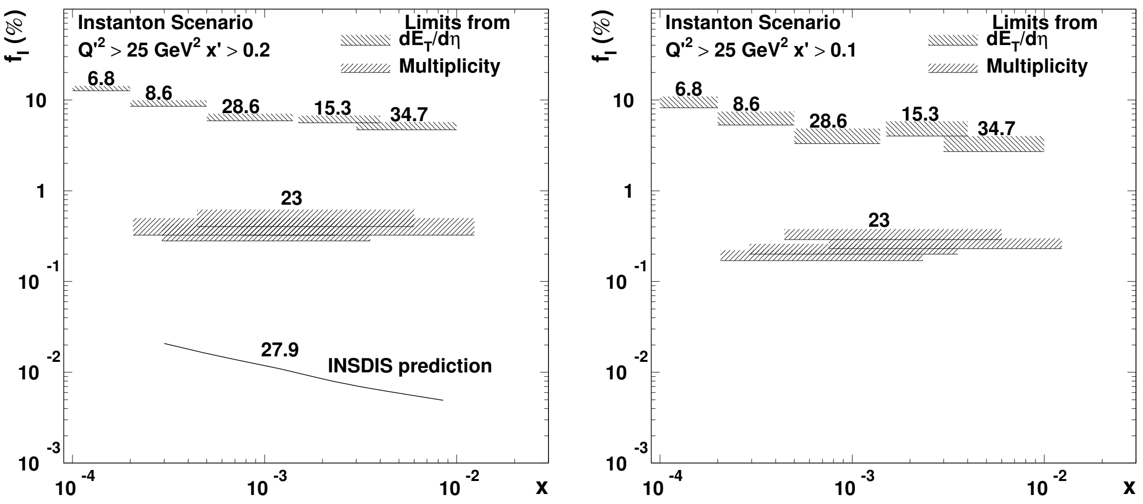

Figure 6: The maximally allowed fraction $f_{\rm lim}$ of instanton induced events in DIS for a) $Q'^2 > 25$ GeV^2 and $x' > 0.2$ and b) $Q'^2 > 25$ GeV^2 and $x' > 0.1$ from transverse energy flows and the multiplicity distribution as function of x. Regions above the lines are excluded at 95% C.L.. The numbers give the average Q^2 values in GeV^2 for the x bins. The theory prediction for 10 GeV^2 $< Q^2 < 80$ GeV^2 is superimposed (full line).

[6] A. Ringwald and F. Schrempp, DESY 96-125, hep-ph/9607238, Proc. of the Workshop DIS 96 on "Deep Inelastic Scattering and Related Phenomena", Rome 1996, eds. G. D'Agostini and A. Nigro, p. 481.

[7] M. Gibbs, T. Greenshaw, D. Milstead, A. Ringwald and F. Schrempp, Proc. of the Workshop on "Future Physics at HERA", Hamburg 1996, eds. G. Ingelman, A. DeRoeck and R. Klanner, vol. 1, p. 509.

[8] S. Moch, A. Ringwald and F. Schrempp, DESY 96-202 hep-ph/9609445 and in prep.

[9] A. Ringwald and F. Schrempp, DESY 96-203, hep-ph/9610213, to appear in the Proc. IXth Int. Sem. "Quarks 96", Yaroslavl, Russia, 1996.

[10] S. Moch, A. Ringwald and F. Schrempp, DESY 97-114, hep-ph/9706400, to appear in the Proc. of the DIS97 workshop, Chicago 1997, eds. J. Repond and D. Krakauer.

[11] H1 Collab., S. Aid et al., Nucl. Phys. B480 (1996) 3.

[12] H1 Collab., S. Aid et al., Z. Phys. C72 (1996) 573.

[13] H1 Collab., S. Aid et al., Phys. Lett. B356 (1995) 118.

[14] H1 Collab., C. Adloff et al., Nucl. Phys. B485 (1997) 3.

[15] L. Lönnblad, Comp. Phys. Comm. 71 (1992) 15, version used: 4.08 .

[16] G. Gustafson, Ulf Petterson, Nucl. Phys. B306 (1988);
G. Gustafson, Phys. Lett. B175 (1986) 453;
B. Andersson, G. Gustafson, L. Lönnblad, Ulf Petterson, Z. Phys. C43 (1989) 625 .

[17] T. Sjöstrand, Comp. Phys. Comm. 39 (1986) 347; CERN-TH-6488-92 (1992)
T. Sjöstrand and M. Bengtsson, Comp. Phys. Comm. 43 (1987) 367 .

[18] T. Sjöstrand, Comp. Phys. Comm. 39 (1986) 347;
T. Sjöstrand and M. Bengtsson, Comp. Phys. Comm. 43 (1987) 367, and for JETSET 7.3, T. Sjöstrand, CERN-TH-6488-92 (1992) .

[19] N. Brook et al., Proc. of the Workshop on Future Physics at HERA, Hamburg 1996, eds. G. Ingelman, A. DeRoeck and R. Klanner, vol. 2, p. 613.

[20] T. Carli, M. Gibbs, M. Kuhlen, A. Ringwald and F. Schrempp, in preparation (version used: QCDINS 1.4.1).

[21] A. Ringwald and F. Schrempp, DESY 97-115, hep-ph/9706399, to appear in the Proc. of the DIS97 workshop, Chicago 1997, eds. J. Repond and D. Krakauer.

[22] A. Ringwald, Nucl. Phys. B330 (1990) 1;
O. Espinosa, Nucl. Phys. B343 (1990) 310.

[23] G. Marchesini et al.,Comp. Phys. Comm. 67 (1992) 465 .

[24] B.R. Webber, Nucl. Phys. B 238 (1984) 492 .

[25] A.D. Martin, W.J. Stirling and R.G. Roberts, Proc. of the Workshop on Quantum Field Theory and Theoretical Aspects of High Energy Physics, eds. B. Geyer and E.M. Ilgenfritz (1993) p. 11.

[26] H.L. Lai et al., Phys. Rev. D 55 (1997) 1280 .

[27] M. Glück, E. Reya, A. Vogt, Z. Phys. C67 (1995) 433.

[28] A. Blondel et al., Proc. of LEP2 workshop, hep-ph/9601212 .

[29] M.F. Hess, Dissertation, Hamburg University 1996, MPI-PhE/96-16.

[30] H1 Collab., S. Aid et al., Nucl.Phys. B470 (1996) 3.

[31] ZEUS Collab., M. Derrick et al., Z. Phys. C69 (1996) 607; DESY 96-076.